Magnetic Excitation Spectra of Sr_{2}IrO_{4} Probed by Resonant Inelastic X-Ray Scattering: Establishing Links to Cuprate Superconductors

Jungho Kim, D. Casa, M. H. Upton, T. Gog, Young-June Kim, J. F. Mitchell, M. van Veenendaal, M. Daghofer, J. van den Brink, G. Khaliullin, and B. J. Kim

Phys. Rev. Lett. **108**, 177003 — Published 23 April 2012

DOI: 10.1103/PhysRevLett.108.177003

Magnetic Excitation Spectra of Sr_2IrO_4 Probed by Resonant Inelastic X-ray Scattering: Establishing Links to Cuprate Superconductivity

Jungho Kim,[1] D. Casa,[1] M. H. Upton,[1] T. Gog,[1] Young-June Kim,[2] J. F. Mitchell,[3]
M. van Veenendaal,[1,4] M. Daghofer,[5] J. van den Brink,[5] G. Khaliullin,[6] B. J. Kim[3]
[1]*Advanced Photon Source, Argonne National Laboratory, Argonne, Illinois 60439, USA*
[2]*Department of Physics, University of Toronto, Toronto, Ontario, Canada M5S 1A7*
[3]*Material Science Division, Argonne National Laboratory, Argonne, IL 60439, USA*
[4]*Department of Physics, Northern Illinois University, De Kalb, IL 60115, USA*
[5]*Institute for Theoretical Solid Sate Physics, IFW Dresden, Helmholtzstr. 20, 01069 Dresden, Germany and*
[6]*Max Planck Institute for Solid State Research, Heisenbergstrae 1, D-70569 Stuttgart, Germany*

We used resonant inelastic x-ray scattering to reveal the nature of magnetic interactions in Sr_2IrO_4, a 5*d* transition-metal oxide with a spin-orbit entangled ground state and $J_{\rm eff}$=1/2 magnetic moments. The magnon dispersion in Sr_2IrO_4 is well described by an antiferromagnetic Heisenberg model with an effective spin one-half on a square lattice, which renders the low-energy effective physics of Sr_2IrO_4 much akin to that in superconducting cuprates. This point is further supported by the observation of exciton modes in Sr_2IrO_4, whose dispersion is strongly renormalized by magnons, which can be understood by analogy to hole propagation in the background of antiferromagnetically ordered spins in the cuprates.

PACS numbers: 74.10.+v, 75.30.Ds, 78.70.Ck

Quantum magnetism in transition-metal oxides (TMOs) arises from superexchange interactions among spin moments that depend on spin-orbital configurations in the ground and excited states. The array of magnetism in 3*d* TMOs is now well understood within the framework of Goodenough-Kanamori-Anderson [1], which assumes conservation of spin angular momentum in the virtual charge fluctuations. However, it has been recently realized that strong relativistic spin-orbit coupling (SOC) can drastically modify the magnetic interactions and yield a far richer spectrum of magnetic systems beyond the standard picture. Such is the case in 5*d* TMOs, in which the energy scale of SOC is on the order of 0.5 eV (as compared to ∼10 meV in 3*d* TMOs). For example, A_2IrO_3 (A=Li,Na) is being discussed as a possible realization of the long sought-after Kitaev model with bond-dependent magnetic interactions [2–4]. Furthermore, strong SOC may result in nontrivial band topology to realize exotic topological states of matter with broken time reversal symmetry, such as a topological Mott insulator [5], Weyl semi-metal, or axion insulator [6]. Despite such intriguing proposals, the nature of magnetic interactions in systems with strong SOC remains experimentally an open question.

In this Letter, we report on the magnetic interactions in a 5*d* TMO, Sr_2IrO_4, with spin-orbit entangled ground state carrying $J_{\rm eff}$=1/2 moments [7, 8], probed by resonant inelastic x-ray scattering (RIXS). These $J_{\rm eff}$=1/2 moments are distinct from pure spins, because their interactions are predicted to depend strongly on lattice and bonding geometries [2] due to admixture of spatially anisotropic orbital moments in the $J_{\rm eff}$=1/2 wavefunction. In the particular case of corner sharing oxygen octahedra on a square lattice, relevant to Sr_2IrO_4 [9](Fig. 1(a)), the magnetic interactions of $J_{\rm eff}$=1/2 moments are described by a pure Heisenberg model, barring Hund's coupling that contributes a weak dipolar-like anisotropy term [2, 10]. This is surprising considering that strong SOC typically results in anisotropic magnetic couplings that deviate from the pure Heisenberg-like spin interaction in the weak SOC limit. A compelling outcome is that a novel Heisenberg antiferromagnet can be realized in the strong SOC limit, on which a novel platform for high temperature superconductivity (HTSC) may be designed.

In the last few years RIXS has become a powerful tool to study magnetic excitations [11]. We report measurement of single magnons using hard x-rays, which has complementary advantages over soft x-rays as detailed later on. The RIXS measurements were performed using the spectrometer at the 9-1D and the MERIX spectrometer at the 30-ID beamline of the Advanced Photon Source. A horizontal scattering geometry was used with the π-polarized incident photons. A spherical diced Si(844) analyzer was used. The overall energy and momentum resolution of the RIXS spectrometer at the Ir L_3 edge (≈11.2 keV) was ≈130 meV and ±0.032 $\AA^{-1}$, respecitvely.

As shown in Fig. 1(b), Sr_2IrO_4 has a canted antiferromagnetic (AF) structure [8] with $T_N \approx 240$ K [12]. Although the 'internal' structure of a single magnetic moment in Sr_2IrO_4, composed of orbital and spin, is drastically different from that of pure spins in La_2CuO_4, a parent insulator for cuprate superconductors, the two compounds share apparently similar magnetic structure. Figures 2(a) and (b) show the dispersion and intensity,

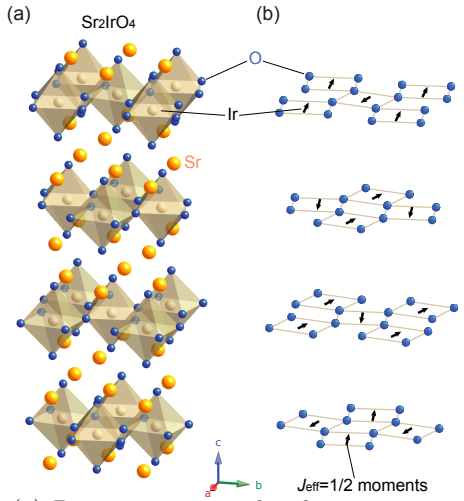

FIG. 1. (a) Due to a staggered in-layer rotation of oxygen octahedra, Sr_2IrO_4 has four IrO_2 layers in the unit cell [9], which coincides with the magnetic unit cell. (b) $J_{\rm eff}$=1/2 moments lie and are canted in the IrO_2 plane [8].

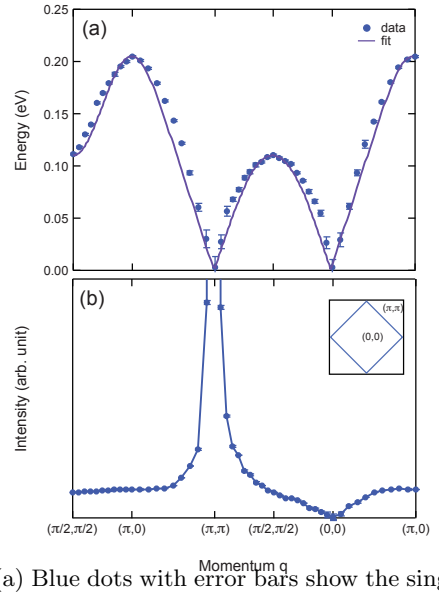

FIG. 2. (a) Blue dots with error bars show the single magnon dispersion extracted by fitting the energy loss curves shown in Fig. 3(b) [13]. The magnons disperse up to ≈205 meV at (π,0) and 110 meV at (π/2,π/2). Solid purple line shows the best fit to the data with J=60, J'=-20, J''=15 meV. (b) Momentum dependence of the intensities showing diverging intensity at (π, π) and vanishing intensity at (0,0). Inset shows the Brillouin zone of the undistorted tetragonal (I4/mmm) unit cell (black square) and the magnetic cell (blue square), and the notation follows the convention for the tetragonal unit cell, as, for instance, in La_2CuO_4 .

respectively, of the single magnon extracted by fitting energy distribution curves shown in Fig. 3(a) [13]. We highlight three important observations. First, not only the dispersion but also the momentum dependence of the intensity show striking similarities to those observed in the cuprates (for instance in La_2CuO_4) by inelastic neutron scattering [14]. This provides confidence that the observed mode is indeed a single magnon excitation [15–18]. Using hard x-ray RIXS allows mapping of an entire Brillouin zone within only a few degrees of 90° scattering geometry so that the spectrum reveals the intrinsic dynamical structural factor with minimal RIXS matrix element effects. Second, the measured magnon dispersion relation strongly supports the theories predicting that the superexhange interactions of $J_{\rm eff}$=1/2 moments on a square lattice with corner-sharing octahedra are governed by a SU(2) invariant Hamiltonian with AF coupling [2, 10]. Third, the magnon mode in Sr_2IrO_4 has a bandwidth of ∼200 meV as compared to ∼300 meV in La_2CuO_4 [14] and $Sr_2CuO_2Cl_2$ [19], which is consistent with energy scales of hopping t and on-site Coulomb energy U in Sr_2IrO_4 being smaller by roughly 50% than those reported for the cuprates [10, 20, 21].

For a quantitative description, we have fitted the magnon dispersion using a phenomenological J-J'-J'' model [22]. Here, the J, J', and J'' correspond to the first, second, and third nearest neighbors, respectively. In this model, the downward dispersion along the magnetic Brillouin zone from (π,0) to (π/2, π/2) is accounted for by a ferromagnetic J' [14, 22]. We find J=60, J'=-20, and J''=15 meV. The nearest neighbor interaction J is smaller than found in cuprates by roughly 50%. The fit can be improved by including higher order terms from longer-range interactions, which were also found to be important in the case of $Sr_2CuO_2Cl_2$ [19]. However, here we do not pursue this path because, as we show below, another kind of magnetic mode in Sr_2IrO_4, which is not present in cuprates, may affect the magnon dispersion.

Characterizing the magnon mode is important because it strongly renormalizes the dispersion of a doped hole/electron and is believed to provide a pairing mechanism for HTSC. We now show that Sr_2IrO_4 supports an exciton mode, which gives access to the dynamics of a particle propagating in the background of AF ordered moments even in an undoped case. Figures 3(a) and (b) show the energy loss spectra along high symmetry directions. No corrections to the raw data such as normalization or subtraction of the elastic contaminations have been made. Another virtue of using hard x-ray is that by working in the vicinity of 90° scattering geometry elastic (Thompson) scattering can be strongly suppressed. In addition to the low-energy magnon branch ($\leq$ 0.2 eV), we observe high-energy excitations with strong momentum dependence in the energy range of 0.4∼0.8 eV. This mode is superimposed on top of a continuum generated by particle-hole excitations across the Mott gap [23](estimated to be ≈0.4 eV from optical spectroscopy [24]). This is schematically shown in Fig. 3(c). Taking the second derivative of the raw data de-emphasizes the intensity arising from the particle-hole continuum and reveals a clear dispersive feature above 0.4 eV, as shown in Fig. 4(a). The energy scale of this

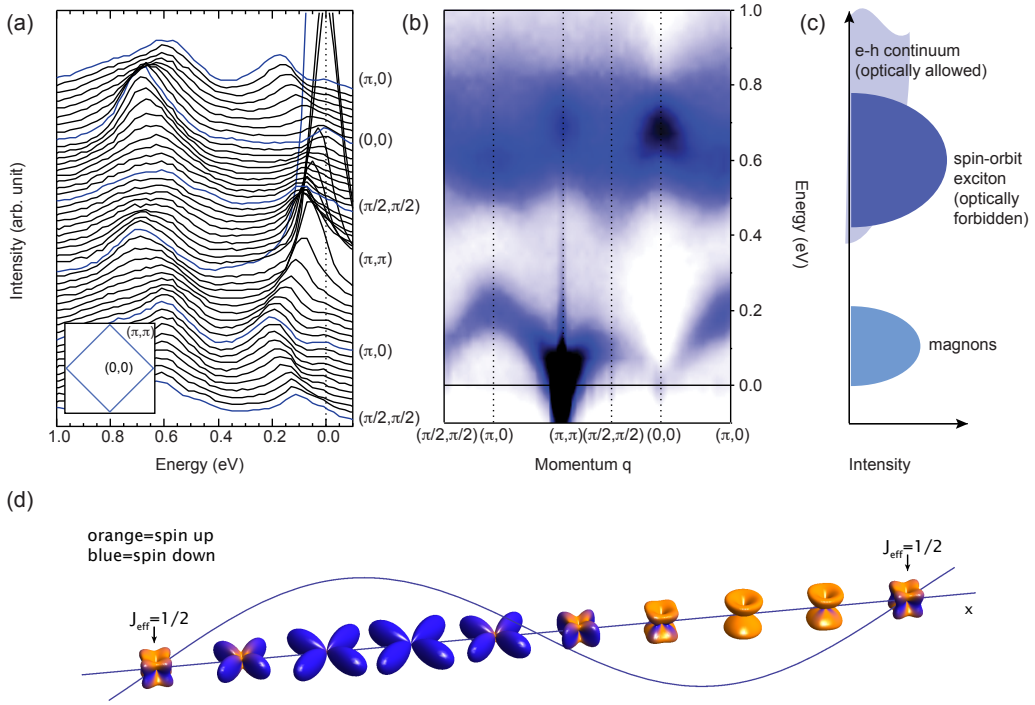

FIG. 3. (a) Energy loss spectra recorded at T=15 K, well below the $T_N \approx 240$ K [8, 12], along a path in the constant L=34 plane. The path was chosen to avoid the magnetic Bragg peaks, which appear at two of the four corners of the unfolded unit cell (black square) shown in the inset (where the same conventions as in Fig. 2 are used). (b) Image plot of the data shown in (a). (c) Schematic of the three representative features in the data. (d) A real space description of the spin-orbit exciton mode.

excitation coincides with the known energy scale of spin-orbit coupling in Sr_2IrO_4 ($\zeta_{SO} \sim 0.5$ eV) [7], and thus we assign it to intra-site excitations of a hole across the spin-orbit split levels in the t_{2g} manifold, *i.e.* from the $J_{\rm eff}$=1/2 level to one of $J_{\rm eff}$=3/2 quartet levels [7, 13, 15] (see Fig. 4(d)). We refer to such an excitation as 'spin-orbit exciton' (Fig. 4(d) [25].

The dispersion of spin-orbit exciton with a bandwidth of at least 0.3 eV implies that this local excitation can propagate coherently through the lattice. Our model of the spin-orbit exciton starts from a recognition that the hopping process is formally analogous to the problem of a hole propagating in the background of AF ordered moments, which has been extensively studied in the context of cuprate HTSC [26]. Although the spin-orbit exciton does not carry a charge, its hopping creates a trail of misaligned spins and thus is subject to the same kind of renormalization by magnons as that experienced by a doped hole [27]. It is well known that the dispersion of a doped hole in cuprates has a minimum at (π/2,π/2) [28], i.e., at the AF magnetic Brillouin zone boundary. Since Sr_2IrO_4 has a similar magnetic order [8], it can be understood by analogy that the dispersion of the spin-orbit exciton should also have its minimum at (π/2,π/2).

The overall bandwidth is determined by the parameters involved in the hopping process, which is depicted in Fig. 4(d) in the hole picture. It involves moving an excited hole to a neighboring site, which happens in two steps. First, the excited hole in site i hops to a neighboring site j ($t_{3/2}$ process), generating an intermediate state with energy U', which is the Coulomb repulsion between two holes at a site in two different spin-orbital quantum levels. Then, the other hole in site j hops back to site i ($t_{1/2}$ process). Thus, the energy scale of the dispersion is set by $2t_{1/2}t_{3/2}/U'$, which is of the order of the magnetic exchange couplings. In fact, these processes lead to the superexchange interactions responsible for the magnetic ordering, but here they involve both the ground state and excited states of Ir ions.

Technically, the spin-orbit exciton hopping can be described by the following Hamiltonian [13]:

$$H = -\sum_{i,j} W_{i,j}^{\alpha\beta} X_{i\alpha}^{\dagger} X_{j\beta} (b_j^{\dagger} + b_i), \qquad (1)$$

where i indicates the lattice site, b ($b^{\dagger}$) is the magnon annihilation (creation) operator, and X denotes the spin-orbit exciton that carries a quantum number α belonging to the $J_{\rm eff}$=3/2 manifold (see Fig. 4(d)). From this expression, the analogy with the case of a moving hole is apparent; in place of the hopping t for the doped hole, we have an effective spin-orbit hopping matrix W with its overall energy scale set by $W = 2t^2/U$.

The AFM background leads to corrections to the bare dispersion of the spin-orbit exciton, which are due to the

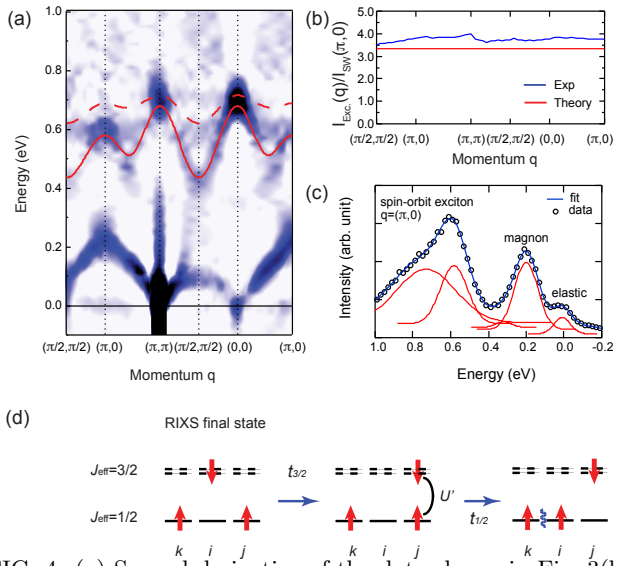

FIG. 4. (a) Second derivative of the data shown in Fig. 3(b), overlaid with the calculation of the dispersion (red solid and dashed lines). W=63 meV was chosen in the calculation, which is within the estimated range [13]. (b) Comparison of the experimental and theoretical integrated spectral weight for the two spin-orbit exciton modes normalized to the single magnon mode at (π,0). (c) Spectrum at (π,0) fitted with five Gaussian peaks. From the right, the peaks (red lines) correspond to elastic, single magnon, two magnon, and two branches of spin-orbit excitons. (d) Schematic of the spin-orbit exciton hopping in the hole representation. By the RIXS process, the hole in the i site is excited to the $J_{\rm eff}$=3/2 quartet. This excited hole hops ($t_{3/2}$ process) to the neighboring site j with the intermediate energy of U'. The other hole in the j site hops back ($t_{1/2}$ process) to the i site, thereby completing the spin-orbit exciton hopping processes and also creating a magnon (blue wavy line).

interaction with magnons and expressed as the self energy

$$\Sigma^{\alpha\beta}_{\mathbf{k}} = -z^2W^2 \sum_{\gamma,\mathbf{q}} \frac{M^{\alpha\gamma}_{\mathbf{k},q} M^{\gamma\beta}_{\mathbf{k},q}}{\omega_{\mathbf{q}}}, \qquad (2)$$

where z is the coordination number and M denotes the vertex [13], using the actual experimental magnon dispersion relation for $\omega_{\mathbf{q}}$ as shown in Fig. 2(a). The only adjustable parameter is W, which only contributes to the overall scaling of the dispersion. The eigenvalues of this 2×2 matrix determine the disperions and correctly captures the main features of the data: the locations of extrema in the dispersion [Fig. 4(a)], nearly momentum independent integrated spectral weight [Fig. 4(b)], and the intensity relative to the magnon intensity [Fig. 4(b,c)].

Our measurement of the spin-orbit exciton dispersion has important implications in modeling 5d transition-metal oxides with strong SOC. First, it shows that not only the $J_{\rm eff}$=1/2 states are localized but also the $J_{\rm eff}$=3/2 states largely retain their atomic-like character. In a contrasting model, in which $J_{\rm eff}$=3/2 states form an itinerant band and only the $J_{\rm eff}$=1/2 states are localized, much akin to the orbital-selective Mott transition scenario [29], one expects to see only a broad electron-hole continuum that results from the independent propagations of a hole and an electron and is much less sensitive to the AF order. Instead, we see the spin-orbit exciton, whose dispersion clearly mirrors the AFM Brillouin zone, coexisting with the particle-hole continuum; a duality of atomic and band nature of the same 5d electrons. Second, the existence of the virtually bound $J_{\rm eff}$=3/2 states only ∼0.5 eV above the ground state implies that the superexchange interactions entail multiorbital contributions. Thus, even for an apparently single orbital $J_{\rm eff}$=1/2 system such as Sr_2IrO_4, the magnetic interactions are multiorbital in character, a fact that must to be taken into account in any quantitative model.

Despite such important differences in the high energy scale, our measurement of the magnon spectrum highlights the similarities with cuprates in the low energy effective physics - a rare realization of "spin" one-half moments on a square lattice with Heisenberg SU(2) invariant interactions and comparable magnon bandwidth. Further, from the observed spin-orbit exciton dispersion, we may expect that a doped hole/electron in Sr_2IrO_4 will display the same dynamics as that observed for a doped hole/electron in the cuprates. The phase diagram of lightly doped Sr_2IrO_4 has just begun to be revealed experimentally [30, 31]. Although superconductivity has not yet been reported, some anomalies that bear strong resemblance to cuprates such as T-linear resistivity have been seen [31, 32]. Only further study will tell if doping can drive Sr_2IrO_4 superconducting.

B. J. K. thanks T. Senthil and H. M. Ronnow for discussions. Work in the Material Science Division and the use of the Advanced Photon Source at the Argonne National Laboratory was supported by the U.S. DOE under Contract No. DE-AC02-06CH11357. Y. K. was supported by the Canada Foundation for Innovation, Ontario Research Fund, and Natural Sciences and Engineering Research Council of Canada. M. vV. was supported by the US Department of Energy (DOE), Office of Basic Energy Sciences, Division of Materials Sciences and Engineering under Award DE-FG02-03ER46097. M. D. acknowledges support by Emmy-Noether program of the the Deutsche Forschungsgemeinschaft (DFG).This work benefited from the RIXS collaboration supported by the Computational Materials Science Network (CMSN) program of the Division of Materials Science and Engineering, Office of Basic Energy Sciences (BES), US DOE under grant number DE-FG02-08ER46540.

[1] J. B. Goodenough, *Magnetism and the Chemical Bond* (Interscience, New York, 1963) p. 1329.
[2] G. Jackeli and G. Khaliullin, Phys. Rev. Lett., **102**,

017205 (2009).
[3] J. Chaloupka, G. Jackeli, and G. Khaliullin, Phys. Rev. Lett., **105**, 027204 (2010).
[4] X. Liu, T. Berlijn, W.-G. Yin, W. Ku, A. Tsvelik, Y.-J. Kim, H. Gretarsson, Y. Singh, P. Gegenwart, and J. P. Hill, Phys. Rev. B, **83**, 220403 (2011).
[5] D. Pesin and L. Balents, Nat. Phys., **6**, 376 (2010).
[6] X. Wan, A. M. Turner, A. Vishwanath, and S. Y. Savrasov, Phys. Rev. B, **83**, 205101 (2011).
[7] B. J. Kim, H. Jin, S. J. Moon, J.-Y. Kim, B.-G. Park, C. S. Leem, J. Yu, T. W. Noh, C. Kim, S.-J. Oh, J.-H. Park, V. Durairaj, G. Cao, and E. Rotenberg, Phys. Rev. Lett., **101**, 076402 (2008).
[8] B. J. Kim, H. Ohsumi, T. Komesu, S. Sakai, T. Morita, H. Takagi, and T. Arima, Science, **323**, 1329 (2009).
[9] M. K. Crawford, M. A. Subramanian, R. L. Harlow, J. A. Fernandez-Baca, Z. R. Wang, and D. C. Johnston, Phys. Rev. B, **49**, 9198 (1994).
[10] F. Wang and T. Senthil, Phys. Rev. Lett., **106**, 136402 (2011).
[11] L. J. P. Ament, M. van Veenendaal, T. P. Devereaux, J. P. Hill, and J. van den Brink, Rev. Mod. Phys., **83**, 705 (2011).
[12] G. Cao, J. Bolivar, S. McCall, J. E. Crow, and R. P. Guertin, Phys. Rev. B, **57**, R11039 (1998).
[13] See supplementary material for details.
[14] R. Coldea, S. M. Hayden, G. Aeppli, T. G. Perring, C. D. Frost, T. E. Mason, S.-W. Cheong, and Z. Fisk, Phys. Rev. Lett., **86**, 5377 (2001).
[15] L. J. P. Ament, G. Khaliullin, and J. van den Brink, Phys. Rev. B, **84**, 020403(R) (2011).
[16] L. J. P. Ament, G. Ghiringhelli, M. M. Sala, L. Braicovich, and J. van den Brink, Phys. Rev. Lett., **103**, 117003 (2009).
[17] M. W. Haverkort, Phys. Rev. Lett., **105**, 167404 (2010).
[18] L. Braicovich, J. van den Brink, V. Bisogni, M. M. Sala, L. J. P. Ament, N. B. Brookes, G. M. D. Luca, M. Salluzzo, T. Schmitt, V. N. Strocov, and G. Ghiringhelli, Phys. Rev. Lett., **104**, 077002 (2010).
[19] M. Guarise, B. D. Piazza, M. M. Sala, G. Ghiringhelli, L. Braicovich, H. Berger, J. N. Hancock, D. van der Marel, T. Schmitt, V. N. Strocov, L. J. P. Ament, J. van den Brink, P.-H. Lin, P. Xu, H. M. Rønnow, and M. Grioni, Phys. Rev. Lett., **105**, 157006 (2010).
[20] H. Jin, H. Jeong, T. Ozaki, and J. Yu, Phys. Rev. B, **80**, 075112 (2009).
[21] H. Watanabe, T. Shirakawa, and S. Yunoki, Phys. Rev. Lett., **105**, 216410 (2010).
[22] We do not include the cyclic exchange J_C because magnons cannot distinguish between ferromagnetic J' and J_C. See, for example, Ref. 33.
[23] K. Ishii, I. Jarriage, M. Yoshida, K. Ikeudhi, J. Mizuki, K. Ohashi, T. Takayama, J. Matsuno, and H. Takagi, Phys. Rev. B, **81**, 115121 (2011).
[24] S. J. Moon, H. Jin, W. S. Choi, J. S. Lee, S. S. A. Seo, J. Yu, G. Cao, T. W. Noh, and Y. S. Lee, Phys. Rev. B, **80**, 195110 (2009).
[25] T. M. Holden, W. J. L. Buyers, E. C. Svensson, R. A. Cowley, M. T. Hutchings, D. Hukin, and R. W. H. Stevenson, J. Phys. C, **4**, 2127 (1971).
[26] P. A. Lee, N. Nagaosa, and X.-G. Wen, Rev. Mod. Phys., **78**, 17 (2006).
[27] S. Schmitt-Rink, C. M. Varma, and A. E. Ruckenstein, Phys. Rev. Lett., **60**, 2793 (1988).
[28] B. O. Wells, Z.-X. Shen, A. Matsuura, D. M. King, M. A. Kastner, M. Greven, and R. J. Birgeneau, Phys. Rev. Lett., **74**, 964 (1995).
[29] V. I. Anisimov, I. A. Nekrasov, D. E. Kondakov, T. M. Rice, and M. Sigrist, Eur. Phys. J. B, **25**, 191 (2002).
[30] O. B. Korneta, T. Qi, S. Chikara, S. Parkin, L. E. D. Long, P. Schlottmann, and G. Cao, Phys. Rev. B, **82**, 115117 (2010).
[31] M. Ge, T. F. Qi, O. B. Korneta, D. E. De Long, P. Schlottmann, W. P. Crummett, and G. Cao, arXiv:1106.2381v1.
[32] H. Okabe, N. Takeshita, M. Isobe, E. Takayama-Muromachi, T. Muranaka, and J. Akimitsu, Phys. Rev. B, **84**, 115127 (2011).
[33] A. M. Toader, J. P. Goff, M. Roger, N. Shannon, J. R. Stewart, and M. Enderle, Phys. Rev. Lett., **94**, 197202 (2005).